NOVEMBER 05 2015

Imaging textural variation in the acoustoelastic coefficient of aluminum using surface acoustic waves

R. Ellwood; T. Stratoudaki; S. D. Sharples; M. Clark; M. G. Somekh

J. Acoust. Soc. Am. 138, 2811–2819 (2015)
https://doi.org/10.1121/1.4934270

Imaging textural variation in the acoustoelastic coefficient of aluminum using surface acoustic waves

R. Ellwood, T. Stratoudaki, S. D. Sharples,[a] M. Clark, and M. G. Somekh[b]
Advanced Optics Group, Faculty of Engineering, University of Nottingham, University Park, Nottingham, NG7 2RD, United Kingdom

(Received 20 April 2015; revised 24 September 2015; accepted 30 September 2015; published online 5 November 2015)

Much interest has arisen in nonlinear acoustic techniques because of their reported sensitivity to variations in residual stress, fatigue life, and creep damage when compared to traditional linear ultrasonic techniques. However, there is also evidence that the nonlinear acoustic properties are also sensitive to material microstructure. As many industrially relevant materials have a polycrystalline structure, this could potentially complicate the monitoring of material processes when using nonlinear acoustics. Variations in the nonlinear acoustoelastic coefficient on the same length scale as the microstructure of a polycrystalline sample of aluminum are investigated in this paper. This is achieved by the development of a measurement protocol that allows imaging of the acoustoelastic response of a material across a samples surface at the same time as imaging the microstructure. The development, validation, and limitations of this technique are discussed. The nonlinear acoustic response is found to vary spatially by a large factor (>20) between different grains. A relationship is observed when the spatial variation of the acoustoelastic coefficient is compared to the variation in material microstructure. © *2015 Acoustical Society of America*.
[http://dx.doi.org/10.1121/1.4934270]

[LC] Pages: 2811–2819

I. INTRODUCTION

Nonlinear acoustic techniques are of interest due to their potential sensitivity to processes such as residual stress,[1–3] fatigue,[4–6] and creep damage[7,8] in materials, where conventional linear techniques are relatively insensitive. A range of nonlinear acoustic techniques[9] exist, all of which probe the third order and higher elastic constants of a material using acoustic waves. This paper focuses on the nonlinear acoustic technique that measures the acoustoelastic effect. The acoustoelastic effect is the change in the velocity of an acoustic wave with the application of stress.[9] This modulation is caused by the inherent nonlinear properties of the material being probed. The acoustoelastic coefficient is a measure of the relative change in velocity with applied stress. The acoustoelastic coefficient is related to both the linear second order elastic constants and the nonlinear third-order and higher elastic constants of a material. The particular elastic constants probed by the acoustoelastic coefficient depends on the type of wave propagated, polarisation of the acoustic wave, and the direction of propagation relative to the applied stress in an anisotropic material.[10] Several methods of determining the acoustoelastic coefficient of a material using ultrasound have been proposed.[11–15] In our previous articles,[16,17] a technique was presented that measures the acoustoelastic coefficient (A_R) by investigating the parametric interaction of surface acoustic waves (SAWs). Dynamic strain, due to the propagation of a SAW, induces stress in the material. Another SAW probes this stress state. The technique produces similar acoustoelastic measurements to a static straining technique.[17] The advantage of this technique is that it allows small ($\sim$0.12 mm^3) localised measurements of the acoustoelastic coefficient using low levels of stress to inspect the material. This ensures that work and damage of the component is avoided during the measurement, a potential problem with high levels of strain used in other techniques.

Most industrially relevant materials, such as metals, are polycrystalline[18] and so consist of multiple randomly orientated grains. The particular third-order elastic constants that affect the propagation of an acoustic wave are dependent on the crystal orientation.[19,20] Variations in the nonlinear acoustic response with a change in propagation direction on crystalline materials has been explored theoretically by various workers.[20,21] Man *et al.*[22] explicitly investigated the effects of texture on the acoustoelastic coefficients. The third-order elastic constants of single crystals were theoretically linked to those of polycrystals by Barsch.[23] Experimental measurements of third-order elastic constants on single crystal aluminum have been conducted by various workers.[19,24] Experimental measurements of the variation in nonlinear response with change in angle of propagation have been made on crystalline silicon by Lomonosov *et al.*[25] Imanishi *et al.*[26] found large variation in the global acoustoelastic coefficient with a change in angle of measurement relative to the rolling direction (and so anisotropy) in polycrystalline aluminum. Wormley *et al.*[27] investigated polycrystalline aluminum with surface skimming longitudinal, shear horizontal and Rayleigh waves and found significant variation in the measurement of the global acoustoelastic coefficients due to

[a]Electronic mail: steve.sharples@nottingham.ac.uk
[b]Current address: Department of Electronic and Information Engineering, The Hong Kong Polytechnic University, Hong Kong.

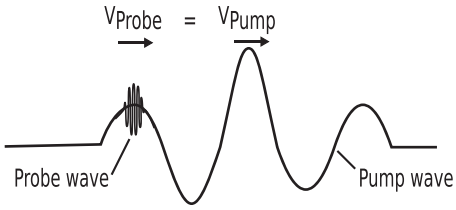

FIG. 1. Diagram depicting the probe-pump wave interaction. As both the probe and pump wave have similar velocities this means that the probe wave only interacts with a single temporal region on the pump wave. The position of the probe wave can be moved relative to the pump wave so that it interacts with regions of different applied stress.

a change in texture (and so microstructure) in the material with respect to rolling direction. Spatially resolved variation in the local stress field, attributed to microstructure, has been imaged using a shear wave birefringence technique by Landa *et al.*[28]

From the existing literature, it is clear that when investigating the acoustoelastic coefficient of materials, variation due to the microstructure is important. The ability to resolve the localised variation in the acoustoelastic coefficient over a region would allow the impact of microstructure to be investigated. It might also potentially offer deeper insight into localised variations due to a range of processes (creep, fatigue, or residual stress), allowing these processes to be better understood.

This paper has two goals. The first is to demonstrate the *imaging of the acoustoelastic coefficient* across a material surface. The second is to investigate the *variation in the acoustoelastic coefficient* within separately resolvable regions of microstructure on an aluminum sample.

In Sec. II the experimental configuration is described, along with the data acquisition and data processing methods developed in order to allow imaging of the acoustoelastic coefficient (see Sec. II E). The repeatability of the developed imaging technique is demonstrated on an aluminum 2024-T351 sample in Sec. II G. Experimental results are given in Sec. III, which presents the variation in the acoustoelastic coefficient on two different but adjacent regions of microstructure of a sample of aluminum, specially produced as described in Ref. 29 to have a large microstructure. Finally, a discussion of this technique, its capabilities and limitations are given in Sec. IV.

II. EXPERIMENTAL METHOD AND INSTRUMENTATION

The dynamic strain technique used in this paper employs the collinear mixing of surface acoustic waves: a high frequency, laser generated probe wave[16] and a low frequency, transducer generated pump wave. Section II A describes the generation of the high frequency probe wave. Section II B describes the generation of the low frequency pump wave that stresses the material as it propagates. The waves co-propagate and interact due to material nonlinearity. Both waves are detected using optical techniques. The probe wave packet is relatively short (<0.25 the period of the pump wave) compared to the period of the pump wave. Both waves are Rayleigh waves, which are non-dispersive provided the sample is sufficiently thick. Consequently, both waves have same base velocities. This means that the probe wave packet interacts with the same region of the pump wave throughout its propagation and therefore experiences a constant and near uniform stress state, see Fig. 1. By controlling the precise timing of the generation of each wave, the probe wave can be made to interact with different temporal points on the pump wave. The system to control the interaction of the two waves is outlined in Sec. II C. As the probe wave interacts with different points on the pump wave, it will experience different stress levels, resulting in the velocity of the probe wave being modulated by different amounts, due to the acoustoelastic effect. The process of converting the received time traces into measurements of the acoustoelastic coefficient (A_R) is described in Sec. II D. Finally the development of an imaging protocol is described in Sec. II E. Figure 2 is a functional schematic of the dynamic strain system.

A. Probe SAW generation and detection

The probe wave, a high frequency SAW, was generated by thermoelastic laser generation. A Q-switched Nd:YAG yttrium

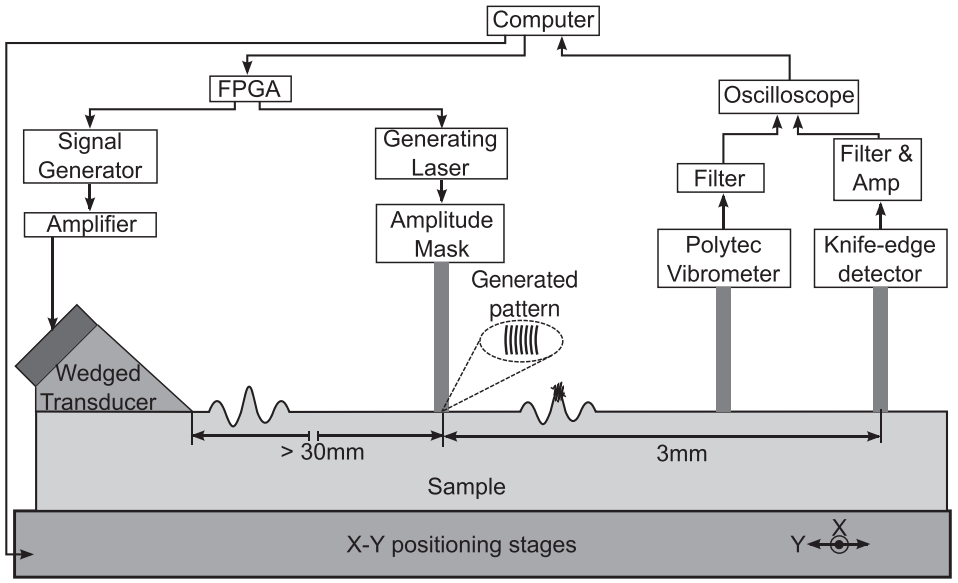

FIG. 2. Dynamic strain experimental configuration. The probe wave is generated by the laser and amplitude mask (see Sec. II A). The pump wave is generated by the signal generator, amplifier, and wedge transducer (see Sec. II B). The probe wave is detected by custom knife-edge detector and the pump wave is detected by a Polytec vibrometer. The timing of the generation of the two waves is controlled by the FPGA (see Sec. II C). The generated waves propagate left to right in the diagram.

aluminum garnet laser ($\lambda = 1064$ nm) with a 10 ns pulse width was used as the source. The beam of the laser was patterned using a grating consisting of concentric arcs which were imaged into a 1 mm^2 area on the sample, producing a wave with a period of 45 μm. A pattern was used to focus and maximize the selected frequency of the acoustic waves generated.[30] The pattern generated a SAW wave with a central frequency of ~68 MHz on aluminum. The SAW came to focus 3 mm from the generation region. A high probe wave frequency was used because this results in a larger phase change in the probe wave for a given stress, which improves the signal to noise ratio provided the noise component of the phase measurement remains small. Also the greater the difference in frequency between the pump (1 MHz) and probe wave, the closer it is to the approximation used in the processing that the probe wave experiences only in-plane components from the strain field of the pump wave[16,17,31] (see Sec. II D).

The probe wave was detected using a custom knife-edge split (beam deflection) detector with a broadband response (400 kHz → 300 MHz).[32,33] Optical generation and detection of the probe wave allowed a compact and spatially localized region to be investigated. The ability to investigate a compact spatial region is advantageous because the variation due to microstructure occurs over a small spatial region for the types of material investigated here. The use of optical techniques removed issues with couplant which affect nonlinear acoustic measurements and also facilitated rapid scanning across the surface of the sample.

B. Low frequency pump wave generation and detection

The low frequency, large amplitude wave used to induce a strain field in the sample was generated using a NDT-Tech (A402S-SB) transducer with a central frequency of 1 MHz. A surface acoustic wave was generated by coupling the transducer through an angled wedge. The transducer was bonded to the sample using phenyl salicylate. The transducer wedge was bonded 30 – 100 mm from the imaging region so as to be away from the near field of the pump wave transducer (near field distance is calculated to be 14 mm based on a beam width of 13 mm and a sound speed of ~3000 ms^{-1}). The pump wave transducer was driven by a three cycle sine wave produced by a signal generator that was amplified using a Ritec RPR-4000 gated amplifier. A Polytec vibrometer (OFV-5000 with decoding card DD300, 30 kHz – 24 MHz) was used to measure the absolute ultrasonic displacement caused by the pump wave.

C. Control electronics

As previously discussed at the beginning of Sec. II, the probe wave interacts with the same finite section of the pump wave, due to the short packet length of the probe wave and the similar velocities of the pump and probe waves. The interaction point between the two waves was dependent on the relative spatial position of the pump wave transducer and the laser ultrasonic source generating the probe wave and the relative temporal triggering. When the spatial position of the generation and detection remain constant, varying the triggering time adjusted the position of the probe wave on the pump wave and consequentially the stress experienced by the probe wave. A field programmable gate array (FPGA) was used to control the generation of the two waves using a variable delay sent from the computer. The FPGA had a clock frequency of 100 MHz, giving a timing resolution of 10 ns.

Using an FPGA to control the wave generation also allowed interlaced differential data acquisition to be performed, as described in Refs. 16 and 17. Interlaced differential data acquisition relies on taking alternative measurements from a reference and target state (Fig. 3). By interlacing the acquisition of a reference state [where the pump and probe waves were not interacting, Fig. 3(A)], a target state [where the waves were interacting see Fig. 3(B)], and subtracting the time of arrival of the reference state from the target state, the impact of the environmental variations can be reduced. The interaction points between waves were switched at a rapid rate (30 Hz) so that the experimental conditions between the two measurements were highly correlated. This, in conjunction with a basic temperature control system (keeping the ambient temperature at 19 ± 0.1 °C), reduced the impact of temperature variations on the measurement. Controlling the impact of temperature variation was important as the fractional velocity changes due to the imposed stresses were small, on the order of 10^{-5}. In order to measure these velocity changes with sufficient accuracy the waveforms were averaged many times (>16 000), which took tens of seconds. Environmental factors such as temperature, which will vary during data acquisition, can have a drastic impact on the velocity of a wave (the relationship between SAW velocity and temperature is typically a few ms^{-1} K^{-1}). Implementing this scheme meant that the standard deviation on measured fractional velocity changes was less than 2×10^{-6}.[17]

D. Data processing

Further data processing was required to convert a) the change in arrival time of the target and reference waves into a fractional velocity change and b) the displacement of the

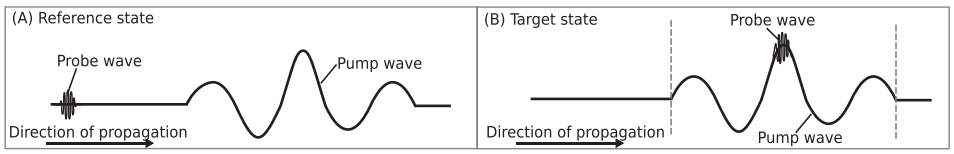

FIG. 3. Diagram demonstrating the interlaced differential data acquisition. By interlacing the acquisition of a reference state [where the pump and probe waves were not interacting (A)], a target state [where the waves were interacting (B)], and subtracting the time of arrival of the reference state from the target state, the impact of the environmental variations can be reduced. Note in the target state the probe wave can interact with the pump wave anywhere in between the two dashed lines.

low frequency wave into a stress. These were both used to determine the acoustoelastic coefficient (A_R).

A full spectrum method[34] was used to determine the difference in propagation time between the arrival of the probe wave at the reference and target states, to give Δt. The full spectrum method determined the delay by cross correlating the approximate delay, then determining the energy weighted slope of the phase at each frequency and least mean squares fitting to it. The distance that the probe wave co-propagated and interacted with the pump wave was kept constant at 3 mm. The difference in the time of the arrival of the probe wave Δt and the time taken for the wave to propagate in the unstressed case, t_0, were used to find the fractional velocity change ($\Delta V/V_0$)

$$\frac{\Delta V}{V_0} = \frac{-\Delta t}{t_0 + \Delta t}. \tag{1}$$

The probe wave had a significantly shorter wavelength (>60 times shorter) than that of the pump wave. According to the theory presented in Viktorov,[31] the out-of-plane particle displacement for a Rayleigh wave is confined to a zone deeper than $0.3\lambda_{\text{acoustic}}$ from the surface. This corresponds to a depth of 0.9 mm from the surface for the low frequency pump wave used here ($\lambda_{\text{acoustic}} = 3$ mm). The in-plane stress is confined to $0.2\lambda_{\text{acoustic}}$ from the surface, while the other stress components approach zero until they reach this depth from the surface. The probe SAW had an acoustic wavelength of 0.04 mm, two orders of magnitude less than the wavelength of the pump wave. This meant that the probe wave energy was confined to the top region of the pump wave where the stress is in-plane only.[16,17,31] The induced stress was calculated from the out-of-plane displacement due to the pump wave. The probe wave packet, T_{probe}, was short compared with the pump wave period, T_{pump}, but its length was still significant. Consequently, the stress value used in the calculation of the acoustoelastic coefficient was taken as the average of the instantaneous stress under the probe wavepacket, weighted by its amplitude. By changing the delay between the generation of the pump and probe waves (and so the point at which they interact) several different stress states are probed. To illustrate this, Fig. 4(A) shows the fractional velocity change (•-•, $\Delta V/V_0$), plotted against the delay between the generation of pump and probe wave on aluminum. The corresponding in-plane stress (σ) experienced by the probe wave, calculated from the out-of-plane displacement caused by the pump wave (+-+) is also plotted on the same figure. Note that both take the form of the pump wave packet as shown in the inset.

The gradient of the linear fit to the fractional velocity change, $\Delta V/V_0$, against stress, σ, is the acoustoelastic coefficient (A_R) $\Delta V/V_0\sigma$ (MPa^{-1}) [see Fig. 4(B)].

E. Imaging of the acoustoelastic coefficient

In order to build up an image it is necessary to measure at many points and it is therefore desirable to minimise the time taken to collect data at each point. The original protocol[16,17] was too slow for imaging, as a single point took 40 min to acquire, due to each measurement consisting of ~60 interactions between the probe and pump wave.

To minimise the time taken for data acquisition, a new protocol was developed. This protocol relied on the assumption that the relation between stress and velocity, and so the acoustoelastic effect, is linear, reducing the number of interactions required for each measurement. This is a reasonable assumption provided the technique is used to investigate materials such as ductile metals that exhibit a classical nonlinearity[3,35,36] and the process remains in the elastic regime. However, this is not true for other materials such as sedimentary rocks, granular materials, materials with cracks or macro-defects, and kinking nonlinear elastic solids that exhibit non-classical hysteretic nonlinearity.[36,37] Consequently this technique is suitable for use with aluminum (investigated in this work) as it exhibits very weak quadratic elasticity, resulting in a velocity change which is linear with strain.[38]

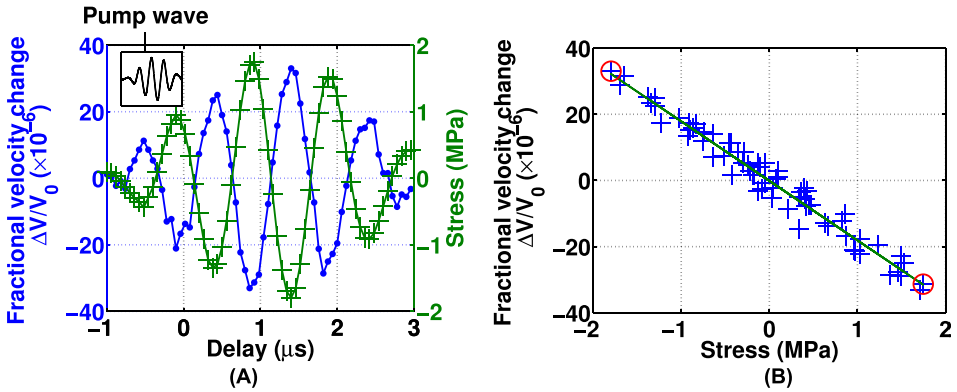

FIG. 4. (Color online) (A) Fractional change in velocity (•-•) against delay value between the generation of the pump and probe wave on aluminum. The stress calculated from the displacement experienced by the packet of the probe wave (+-+). (Inset) trace from the oscilloscope showing the pump wave as it is detected by the Polytec interferometer, illustrating the source of the modulation of the fractional velocity measurement and stress. (B) Fractional velocity change of probe wave plotted against the stress experience by the probe wave packet from (A), the gradient of this plot corresponds to the acoustoelastic coefficient (A_R, in this case -18×10^{-6} MPa^{-1}). The two circles correspond to the points where the maximum and minimum stress is experienced by the probe wave.

For these conditions, only two separate interactions at separate stress states were needed to measure the acoustoelastic coefficient. This reduces the amount of time taken to acquire a single point measurement to 40 s (~sixty times faster than measurements using the previous protocol). As a result imaging of the A_R over the surface of a sample by raster scanning an area became practical. The technique was implemented by placing the sample on a set of long travel computer controlled stages (300 mm PI M-531.DD with 0.1 μm linear encoders) and raster scanning the sample in the x-y plane.

The optimum interaction points of the probe and pump SAWs were those where the stresses were at a maximum and minimum [see Fig. 4(B)]. Imaging the acoustoelastic coefficient over a 16 mm^2 area took approximately 18 h.

The timing of the generation of the probe and pump wave was arranged so that the probe wave interacted with the peak and trough of the pump wave at each spatial location, corresponding to the maximum positive and negative stress (see Fig. 5).

F. Imaging the linear acoustic properties with SRAS

The area that was to be acoustoelastically imaged was first scanned using a technique called spatially resolved acoustic spectroscopy (SRAS).[32,39] SRAS is a linear acoustic technique that measures the linear velocity of a propagating wave. The linear velocity of an acoustic wave is sensitive to the second order elastic constants of a material only. When used on polycrystalline materials, such as a metal, the measured velocity of the propagating wave is determined by the underlying microstructure at the point of generation of the wave. In this way, the SRAS technique produces a linear acoustic velocity map which gives an image of the microstructure of the material.

Performing a SRAS scan before measuring the acoustoelastic coefficient has two benefits. The first benefit is that any variation in the acoustoelastic coefficient of the material can be compared to the underlying microstructure of the material. The second benefit of using SRAS is that it provides an image based on the material structure with which to relocate the sample, even if it has been removed and reinstalled into the system. The area inspected acoustoelastically was selected to have easily identifiable microstructure so as to aid with relocation. The advantage of using the SRAS technique over other techniques that can image the microstructure of the material (for example, electron backscatter diffraction[40]) was that the same experimental configuration used to measure the acoustoelastic coefficient of the material could be used to generate a SRAS image.

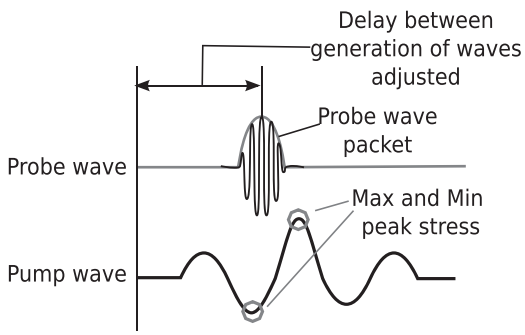

FIG. 5. Diagram depicting the adjustment of the delay between the generation of the probe wave and the pump wave, so that the probe wave interacts with portions of the pump wave that correspond to experiencing the maximum and minimum stress.

A SRAS image was generated by scanning across the sample surface while producing and recording a series of surface acoustic waves using the probe wave system used in the acoustoelastic measurement. A laser generated SAW was generated with a fixed arc grating, giving the SAW a similar wavelength. As the linear acoustic velocity of the material under the generation region varied, the frequency of the generated wave also varied. By measuring the frequency of the generated acoustic wave and knowing the period of the grating, the local velocity of the sample could be determined. No pump wave was produced during the SRAS measurement as it was a purely linear measurement.

G. Repeatability of imaging the acoustoelastic coefficient

The acoustoelastic imaging technique developed in section 2.5 allows the monitoring of the acoustoelastic coefficient (A_R) over an area. In this section initial images of the acoustoelastic variation on aluminum 2024-T351 are presented. The typical grain size was in the region of 20–40 μm as determined by a high resolution SRAS scan. The aluminum sample was machined and polished to give an optically smooth finish. The sample was scanned over a square area of 16 mm^2.

The resultant image of the acoustoelastic coefficient across the sample can be seen in Fig. 6(A). The pump SAW propagated from left to right. The scan area was acquired in the order left to right, top to bottom. The range of A_R shows a distinct spatial variation that is present in the image shown in Fig. 6(A). The signal to noise ratio [see Fig. 6(C)] gave an indication as to the certainty in the measurement of the fractional velocity change. Points with a poor signal to noise ratio (below 5) were excluded from the final acoustoelastic image. The SRAS linear velocity map [see Fig. 6(B)] is also shown to illustrate the variation in the microstructure in the imaged region.

To validate the images taken and prove the repeatability of the technique, a second acoustoelastic image of the area originally scanned was taken after the sample had been removed and reinstalled into the system (relocated using registration marks on the sample itself and cross-correlation of SRAS images). In Figs. 7(A) and 7(B) the SRAS velocity data for each area are compared. A good correlation was seen in the velocity data, which relates to the microstructure. This indicates the second area imaged was in the same region as the first area imaged to within the resolution of the SRAS scan (100 μm) and demonstrated the accuracy in the re-positioning of the samples. The acoustoelastic images can be seen in Figs. 7(C) and 7(D).

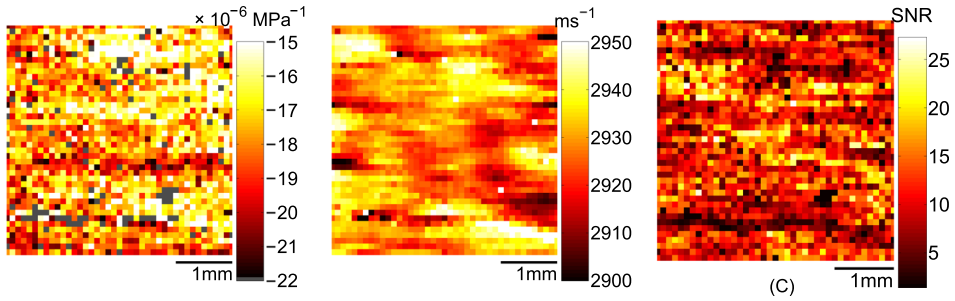

FIG. 6. (Color online) Initial measurements of the acoustoelastic coefficient (A_R). (A) Image of acoustoelastic coefficient across aluminum sample, A_R (MPa^{-1}), any gray areas correspond to regions where the signal to noise ratio was below an arbitrary level of 5. (B) Image of linear SAW velocity (SRAS, ms^{-1}), for the area corresponding to the region over which acoustoelastic image was taken. The velocity variation denotes a change in underlying microstructure. (C) Image of signal to noise ratio of the probe wave.

Again the range of A_R shows a distinct spatial variation that is present in both images seen in Figs. 7(C) and 7(D). Grey regions in 7(C) and 7(D) correspond to regions of low signal to noise ratio (SNR, arbitrary level of 5). The areas of low SNR are spatially correlated between the two measurements due to them corresponding to regions of poor surface quality. A good correlation is seen between the two acoustoelastic coefficient images. The correlation between two variables can be quantified by the Pearson product moment correlation.[41] The Pearson correlation coefficient, R, is dimensionless with a value ranging between −1 and +1. The closer the coefficient is to 1 or −1 the better the correlation between the two variables. In this case the Pearson correlation coefficient between the two acoustoelastic images was 0.81. This was a good correlation value and shows that the observed variation in the acoustoelastic property was spatially repeatable over the surface of the sample. A_R varies in the first image between −6.6 and -22.5×10^{-6} MPa^{-1} (71%) and between −11.1 and -25.4×10^{-6} MPa^{-1} (56%) for the second image. As the variation in the measurement is spatially repeatable and the variation is so large, it is clearly important that accurate re-registration of nonlinear measurements takes place.

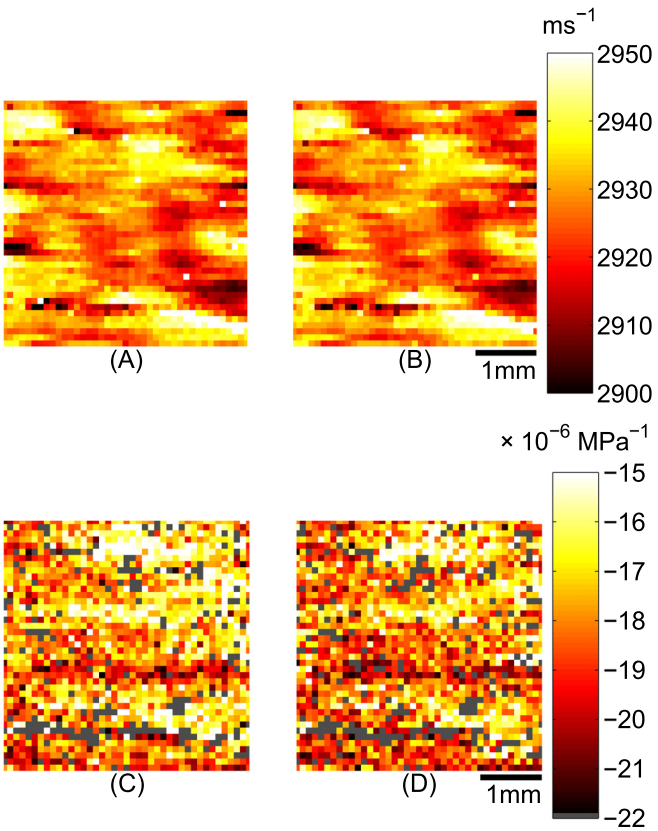

FIG. 7. (Color online) Comparison between two SRAS velocity images between the initial experiment (A) and the repeat (B). A good correlation was seen, indicating good relocation between experiments. The initial acoustoelastic images can be seen in (C) and the repeat in (D). Dark gray areas correspond to areas where the measurement had a low signal to noise ratio. A good correlation between the acoustoelastic images can be seen.

III. EXPERIMENTAL RESULTS

This section describes an experiment that investigated the relationship between the acoustoelastic coefficient of a region and the underlying microstructure. To investigate this relationship, a sample with a microstructure of a similar scale as the resolution of the measurement of A_R (3 mm) was used. This sample was produced following the process detailed in Ref. 29. The resolution of the measurement of A_R was defined by the region over which the pump and probe waves interact.[17] The SRAS technique was used to image the microstructure of the sample [see Fig. 8(A)]. Figure 8(B) shows an image of the acoustoelastic coefficient of the sample. The area over which the acoustoelastic images was taken is shown by the dashed line in Fig. 8(A). It can be seen on the SRAS image [Fig. 8(A)] that there were two grains (one fast, dark, and one slow, light area) along with an interface region between the two. In the acoustoelastic image two separate regions were also observed with a clear

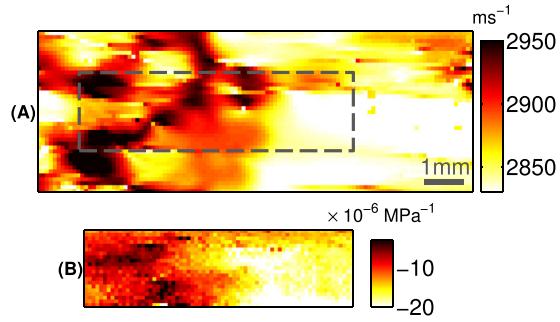

FIG. 8. (Color online) SRAS (A) and acoustoelastic coefficient (B) image taken from a sample of aluminum with a grain size on the order of millimeters. The dotted line in (A) denotes the region over which the acoustoelastic coefficient was mapped.

region between them. The values of A_R vary between -1.0×10^{-6} MPa^{-1} (a relatively linear response) and -22.8×10^{-6} MPa^{-1} (a significantly nonlinear response), which is a large variation (factor of 22) to occur over a relatively small area.

A. SRAS and A_R: Relative inspection regions

To accurately assess the relationship between the microstructure of the sample and the A_R measurements, consideration of the relative inspection regions of the SRAS measurements (known to be related to the underlying microstructure) and the A_R measurements needs to be made. The pump and probe SAWs interacted over a finite length of 3 mm as part of the measurement of A_R. A range of microstructure exists along this interaction region. The SRAS technique was sensitive to a region the size of the generation spot of the probe wave [<1 mm^2, see Fig. 9(A)]. To correctly relate the imaged A_R to the microstructure of the material that the measurement has been taken over, the corresponding linear velocity measurements must be averaged along the interaction region.

The probe SAW was generated using a series of arcs to produce a focused wave. The interaction region between the probe and pump SAWs took the form of a triangle [see Fig. 9(B)]. Averaging the linear velocity over a series of triangular regions gives an indication as to the average structure that the measurement of A_R takes place in, this can be seen in the velocity image seen in Fig. 10(A), the corresponding acoustoelastic data can be seen in Fig. 10(B). The triangularly averaged velocity is plotted against A_R (see Fig. 11). The relationship between the triangularly averaged velocity (representing the microstructure of the sample that the measurement of A_R took place in) and the acoustoelastic coefficient is complex, and not fully defined here. Many other grain orientations would have to be investigated to define this relationship and this is left to future work. However, a correlation between the acoustoelastic measurement and the SRAS measurement is present. This spatial correlation between the two measurements would imply that the variation observed in both is due to the underlying microstructure.

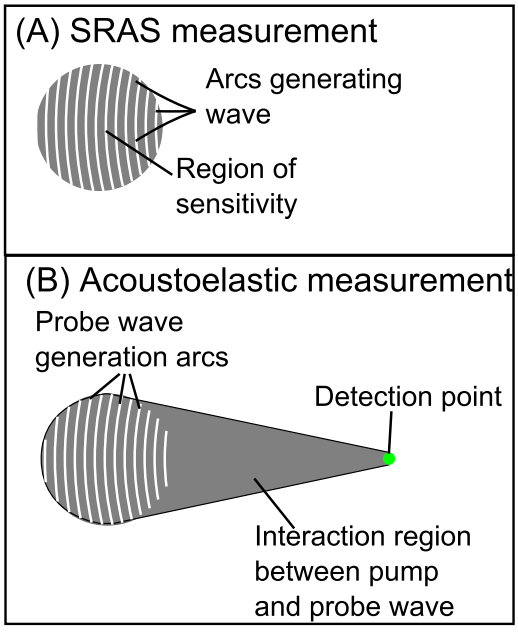

FIG. 9. (Color online) Diagram depicting the relative size of regions of sensitivity for (A) the SRAS measurement and (B) the pump and probe wave as part of the A_R measurement.

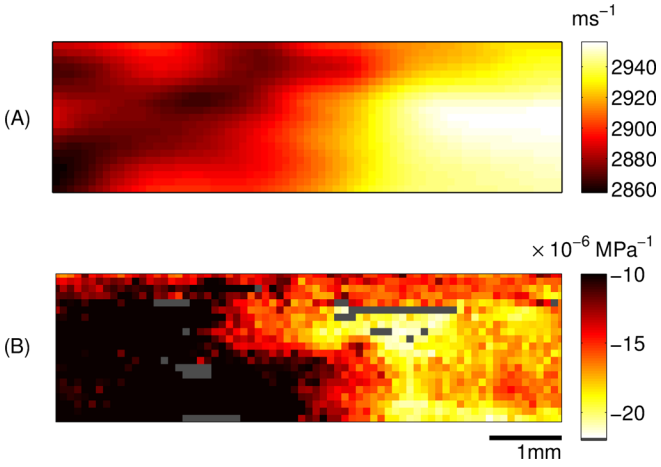

FIG. 10. (Color online) (A) SRAS velocity data averaged over a triangular region with the dimensions of the probe wave as it propagates and interacts with the pump wave before it was detected, for each interaction location. (B) Acoustoelastic image of region corresponding to the spatially averaged SRAS velocity data in (A).

IV. DISCUSSION AND FURTHER WORK

This paper has presented measurements of the acoustoelastic coefficient varying locally on a similar scale as the microstructure of a polycrystalline material. As far as the authors are aware, this is the first time this has been achieved and this was done by developing a novel technique to image the local variation in the acoustoelastic coefficient across a

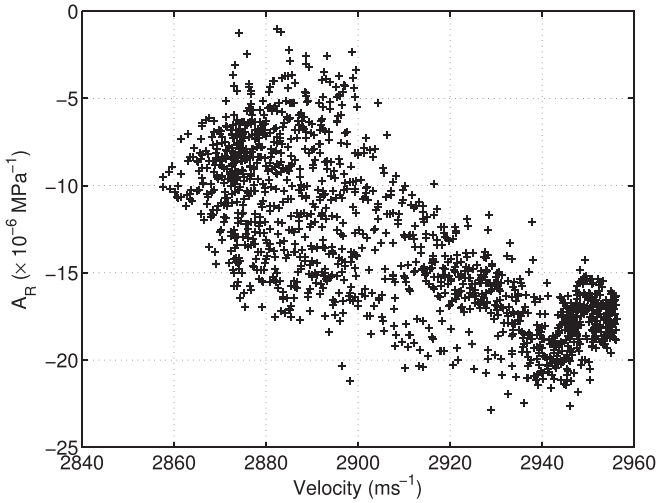

FIG. 11. Plot of the linear velocity taken using the SRAS technique (representing the microstructure of the sample) averaged over a triangular region corresponding to the region that the acoustoelastic coefficient was measured in for each location against the acoustoelastic coefficient. A relationship between the two is evident but more grain orientations would need to be investigated to identify the precise form of the relationship.

sample. The images taken with this system were shown to be highly repeatable on a single sample, with variation seen from sample to sample. The results give high confidence that the variation is due to sample features rather than instrumental effects.

The variation in the measurement of A_R found here is spatially determined and repeatable. The variation is also found to be very large (by a factor of 22). It is clearly important that accurate re-registration of nonlinear measurements should take place, especially when trying to measure complex processes such as residual stress, fatigue, and creep damage in a material.

The imaging technique implemented in this paper relied on the relationship between the change in the stress and the fractional velocity change being linear. While this is true for most metals,[3,35,38] other materials such as granular materials and kinking nonlinear elastic solids do not always demonstrate this trend.[36,37] Instead these materials demonstrate hysteresis in the relationship between fractional velocity change and stress, posing limits to the applicability of the technique developed in this paper.

The developed technique was sensitive to velocity changes on the order of $3-4\,\mathrm{mm\,s^{-1}}$. The largest stress that could be applied by the pump wave using our transducer configuration was on the order of 4 MPa. This gave a maximum sensitivity of this instrument of less than $1\times10^{-6}\,\mathrm{MPa^{-1}}$. Aluminum has an acoustoelastic coefficient on the order of $-15\times10^{-6}\,\mathrm{MPa^{-1}}$, which is relatively large compared to the sensitivity of the instrument. Other materials have smaller acoustoelastic coefficients (titanium, for example, has a nonlinear response of roughly half that of aluminum[42]) and so the current experimental set-up might not be able to observe them. However, there are a range of potential methods to improve the sensitivity of the instrument. The first would be to generate a larger amplitude pump wave. The pump wave used in this experiment has a center frequency of 1 MHz, the availability of transducers capable of producing high frequency waves at larger amplitude is limited making this experimentally difficult to implement at present. However, with the development of transducers for high-intensity focused ultrasound systems, this technological challenge may soon be overcome. An alternative may be to increase the resolution in the timing of the arrival of the probe wave. This is dependent on the availability of suitably high speed oscilloscopes.

This paper explores the nature of the observed variation in the imaged acoustoelastic coefficient by investigating a sample which has a microstructure of the same scale as the measurement of the acoustoelastic coefficient. It was observed that the acoustoelastic coefficient varies over a spatial region on a polycrystalline sample. The variation in grain structure was also mapped using a technique sensitive to the local second order elastic constants, SRAS. The spatial correlation between the SRAS data and the acoustoelastic data indicates that the variation observed in the acoustoelastic coefficient is due to the same mechanism as for the SRAS data, that is, the change in the local microstructure. While the acoustoelastic measurement is primarily a nonlinear ultrasonic technique, the acoustoelastic constant measured is not independent of the linear second order elastic constants. This makes it difficult to decouple the changes in the acoustoelastic measurement purely due to changes in linear contributions (second order elastic constants) and the nonlinear contribution (third order and higher elastic constants). To do this measurements of the wave propagating with the stress applied at several different directions would be required,[10] which is difficult to achieve with this particular experimental configuration. However it should be noted that the linear SRAS measurement varied by a maximum of 3.5% $(2850-2950\,\mathrm{ms^{-1}})$ across the region imaged, while the acoustoelastic measurement varied by up to a factor of 22. The larger proportional change in the acoustoelastic coefficient with a change in grain orientation would indicate that the variation of the nonlinear terms that contribute to the acoustoelastic measurement with grain orientation is significant. Meaning that nonlinear acoustic measurements are highly sensitive to grain orientation. This relationship could be further investigated by probing a larger number of grain orientations. Practically this is best implemented by imaging samples with a smaller microstructure. In order to facilitate the imaging of smaller microstructure, the probe wave frequency could be increased, which would improve the temporal resolution of the measurement. This would allow the co-propagation distance between the pump and probe wave to be reduced without increasing the error in the measurement.

Despite many encouraging early results [43–46] single sample repeatability and sample to sample variation has proved a challenge for nonlinear acoustic techniques. This paper has shown the strong dependence of the microscopic nonlinear parameter on position and the microstructure, indicating that a more reliable measurement system may be constructed either using higher resolutions (giving single grain measurements) or lower resolution (encompassing a sufficiently large sample of the microstructure).

Further proposed work includes investigation into the spatial variation of classical material nonlinearity with fatigue at the stage before macro-dislocations form. Samples that have microstructure considerably smaller–and larger–than those measured here will also be investigated.

ACKNOWLEDGMENTS

This work was supported by the UK RCNDE (Research Centre in Nondestructive Evaluation), and the UK TSB (Technology Strategy Board).

[1]Z. Wei, X. Zhou, and Y. Cheng, "Acoustoelastic determination of local surface stresses in polymethylmethacrylate," Appl. Acoust. **61**, 477–485 (2000).
[2]M. Liu, J. Kim, L. Jacobs, and J. Qu, "Experimental study of nonlinear Rayleigh wave propagation in shot-peened aluminum plates feasibility of measuring residual stress," NDT&E Int. **44**, 67–74 (2011).
[3]D. Crecraft, "The measurement of applied and residual stresses in metals using ultrasonic waves," J. Sound Vib. **5**(1), 173–192 (1967).
[4]P. Nagy, "Fatigue damage assessment by nonlinear ultrasonic materials characterization," Ultrasonics **36**, 375–381 (1998).
[5]K. Abeele, A. Sutin, J. Carmeliet, and P. Johnson, "Micro-damage diagnostics using nonlinear elastic wave spectroscopy (NEWS)," NDT&E Int. **34**, 239–248 (2001).

[6]O. Buck, W. Morris, and J. Richardson, "Acoustic harmonic generation at unbonded interfaces and fatigue cracks," Appl. Phys. Lett. **33**(5), 371–373 (1978).
[7]S. Baby, B. Kowmundi, C. Omprakash, D. Satyanarayana, K. Balasubramaniam, and V. Kumar, "Creep damage assessment in titanium alloy using a nonlinear ultrasonic technique," Scr. Mater. **59**, 818–821 (2008).
[8]T. Ohtani, H. Ogi, and M. Hirao, "Noncontact evaluation of surface-wave nonlinearity for creep damage in CrMoV steel," Jpn. J. Appl. Phys. **48**, 07GD02 (2009).
[9]A. N. Norris, "Finite-amplitude waves in solids," in *Nonlinear Acoustics*, edited by M. F. Hamilton and D. T. Blackstock (Academic Press, San Diego, 1998), pp. 270–274.
[10]M. Duqunnoy, M. Ouaftouh, M. Ourak, and F. Jenot, "Theoretical determination of Rayleigh wave acoustoelastic coefficient: Comparison with experimental values," Ultrasonics **39**, 575–583 (2002).
[11]R. Kumon and D. Hurley, "Effects of residual stress on the thin-film elastic moduli calculated from surface acoustic wave spectroscopy experiments," Thin Solid Films **484**, 251–256 (2005).
[12]B. Mi, J. Michaels, and T. Michaels, "An ultrasonic method for dynamic monitoring of fatigue crack initiation and growth," J. Acoust. Soc. Am. **119**, 74–84 (2006).
[13]M. Kato, T. Sato, and K. Ando, "Determination of the higher-order elastic compliance constants of metals from measurements of the dependence of ultrasound velocity on stress," J. Acoust. Soc. Am. **101**, 2111–2121 (1997).
[14]M. Vila, F. Vander Meulen, S. Dos Santos, L. Haumesser, and O. Bou Matar, "Contact phase modulation method for acoustic nonlinear parameter measurement in solid," Ultrasonics **42**, 1061–1065 (2004).
[15]G. Renaud, S. Callé, and M. Defontaine, "Remote dynamic acoustoelastic testing: Elastic and dissipative acoustic nonlinearities measured under hydrostatic tension and compression," Appl. Phys. Lett. **94**, 011905 (2009).
[16]T. Stratoudaki, R. Ellwood, S. Sharples, M. Clark, and M. Somekh, "Measurement of material nonlinearity using surface acoustic wave parametric interaction and laser ultrasonics," J. Acoust. Soc. Am. **129**, 1721–1728 (2011).
[17]R. Ellwood, T. Stratoudaki, S. Sharples, M. Clark, and M. Somekh, "Determination of the acoustoelastic coefficient for surface acoustic waves using dynamic acoustoelastography: An alternative to static strain," J. Acoust. Soc. Am. **135**, 1064–1070 (2014).
[18]W. Moffat, G. Pearsall, and J. Wulf, *Structure and Properties of Materials* (Wiley, New York, 1964), Vol. 1, Chap. 6, pp. 122–147.
[19]V. Sarma and P. Reddy, "Third-order elastic constants of aluminium," Phys. Status Solidi A **10**(2), 563–567 (1972).
[20]R. Kumon and M. Hamilton, "Effects of harmonic phase on nonlinear surface acoustic waves in the (111) plane of cubic crystals," J. Acoust. Soc. Am. **113**(6), 3060–3064 (2003).
[21]M. Hamilton, Y. LL'inkii, and E. Zabolotskaya, "Nonlinear surface acoustic waves in crystals," J. Acoust. Soc. Am. **105**(2), 639–651 (1999).
[22]C. Man and R. Paroni, "On the separation of stress-induced and texture-induced birefringence in acoustoelasticity," J. Elast. **45**(2), 91–116 (1996).
[23]G. Barsche, "Relation between third-order elastic constants of single crystals and polycrystals," J. Appl. Phys. **39**(8), 3780–3793 (1968).
[24]J. Thomas, "Third-order elastic constants of aluminum," Phys. Rev. **175**(3), 955–962 (1968).
[25]A. Lomonosov, P. Hess, R. Kumon, and M. Hamilton, "Laser-generated nonlinear surface wave pulses in silicon crystals," Phys. Rev. B **69**, 035314 (2004).
[26]E. Imanishi, M. Sasabe, and Y. Iwashimizu, "Experimental study on acoustical birefringence in stressed and slightly anisotropic materials," J. Acoust. Soc. Am. **71**(3), 565–572 (1982).
[27]S. Wormley, R. Thompson, G. Alers, R. Alers, and M. Warchol, "The influence of mircrostructure on the acoustoelastic measurements of stress in aluminium alloys," AIP Conf. Proc. **615**, 1688–1695 (2002).
[28]M. Landa and J. Plesek, "Contrast enhancement of ultrasonic imaging of internal stresses in materials," Ultrasonics **40**, 531–535 (2002).
[29]J. Hernández, M. Clark, S. Sharples, M. Somekh, and V. Lopez, "Aberrations in materials with random inhomogeneities," J. Acoust. Soc. Am. **121**(3), 1396–405 (2007).
[30]M. Clark, S. Sharples, and M. Somekh, "Non-contact acoustic microscopy," Meas. Sci. Technol. **11**, 1792–1801 (2000).
[31]I. Viktorov, *Rayleigh and Lamb Waves: Physical Theory and Applications* (Plenum Press, New York, 1967), pp. 1–7.
[32]R. Smith, W. Li, J. Coulson, M. Clark, M. Somekh, and S. Sharples, "Spatially resolved acoustic spectroscopy for rapid imaging of material microstructure and grain orientation," Meas. Sci. Technol. **25**, 055902 (2014).
[33]C. Scruby and L. Drain, *Laser Ultrasonics Techniques and applications* (Adam Hilger, Bristol, 1990), Chap. 2, pp. 66–70.
[34]J. S. Bendat and A. G. Piersol, *Random Data: Analysis and Measurement Procedures* (Wiley-Interscience, New York, 1971), pp. 31–34.
[35]G. Johnson and W. Springer, "A comparison of measured and predicted second and third-order elastic constants of a textured aggregate," Int. J. Solids Struct. **25**(6), 609–619 (1989).
[36]P. Finkel, A. Zhou, S. Basu, O. Yeheskel, and M. Barsoum, "Direct observation of nonlinear acoustoelastic hysteresis in kinking nonlinear elastic solids," Appl. Phys. Lett. **94**, 241904 (2009).
[37]G. Renaud, S. Rivière, S. Haupert, and P. Laugier, "Anisotropy of dynamic acoustoelasticity in limestone, influence of conditioning, and comparison with nonlinear resonance spectroscopy," J. Acoust. Soc. Am. **133**(6), 3706–3718 (2013).
[38]G. Renaud, M. Talmant, S. Calle, M. Defontaine, and P. Laugier, "Nonlinear elastodynamics in micro-inhomogeneous solids observed by head-wave based dynamic acoustoelastic testing," J. Acoust. Soc. Am. **130** 3583–3589 (2011).
[39]W. Li, S. D. Sharples, R. J. Smith, M. Clark, and M. G. Somekh, "Determination of crystallographic orientation of large grain metals with surface acoustic waves," J. Acoust. Soc. Am. **132**(2), 738–745 (2012).
[40]A. Schwartz, M. Kumar, B. Adams, and D. Field, *Electron Backscatter Diffraction in Materials Science* (Springer, London, 2009), pp. 1–3.
[41]N. Narayanan, *Statistics* (PHL Learning, New Delhi, 2011), pp. 216–217.
[42]X. Jacob, C. Barrière, and D. Royer, "Acoustic nonlinearity parameter measurements in solids using the collinear mixing of elastic waves," Appl. Phys. Lett. **82**(6), 886–888 (2003).
[43]V. Rao, E. Kannan, R. Prakash, and K. Balasubramaniam, "Fatigue damage characterization using surface acoustic wave nonlinearity in aluminum alloy AA7175-T7351," J. Appl. Phys. **104**, 123508 (2008).
[44]J. Blackshire, S. Sathish, J. Na, and J. Frouin, "Nonlinear laser ultrasonic measurements of localised fatigue damage," Rev. QNDE **22**, 1479–1488 (2003).
[45]J. Herrmann, J. Kim, L. Jacobs, J. Qu, J. Littles, and M. Savage, "Assessment of material damage in a nickel-base superalloy using nonlinear Rayleigh surface waves," J. Appl. Phys. **99**, 124913 (2006).
[46]H. Ogi, M. Hirao, and S. Aoki, "Noncontact monitoring of surface-wave nonlinearity for predicting the remaining life of fatigued steels," J. Appl. Phys. **90**(1), 438–442 (2001).